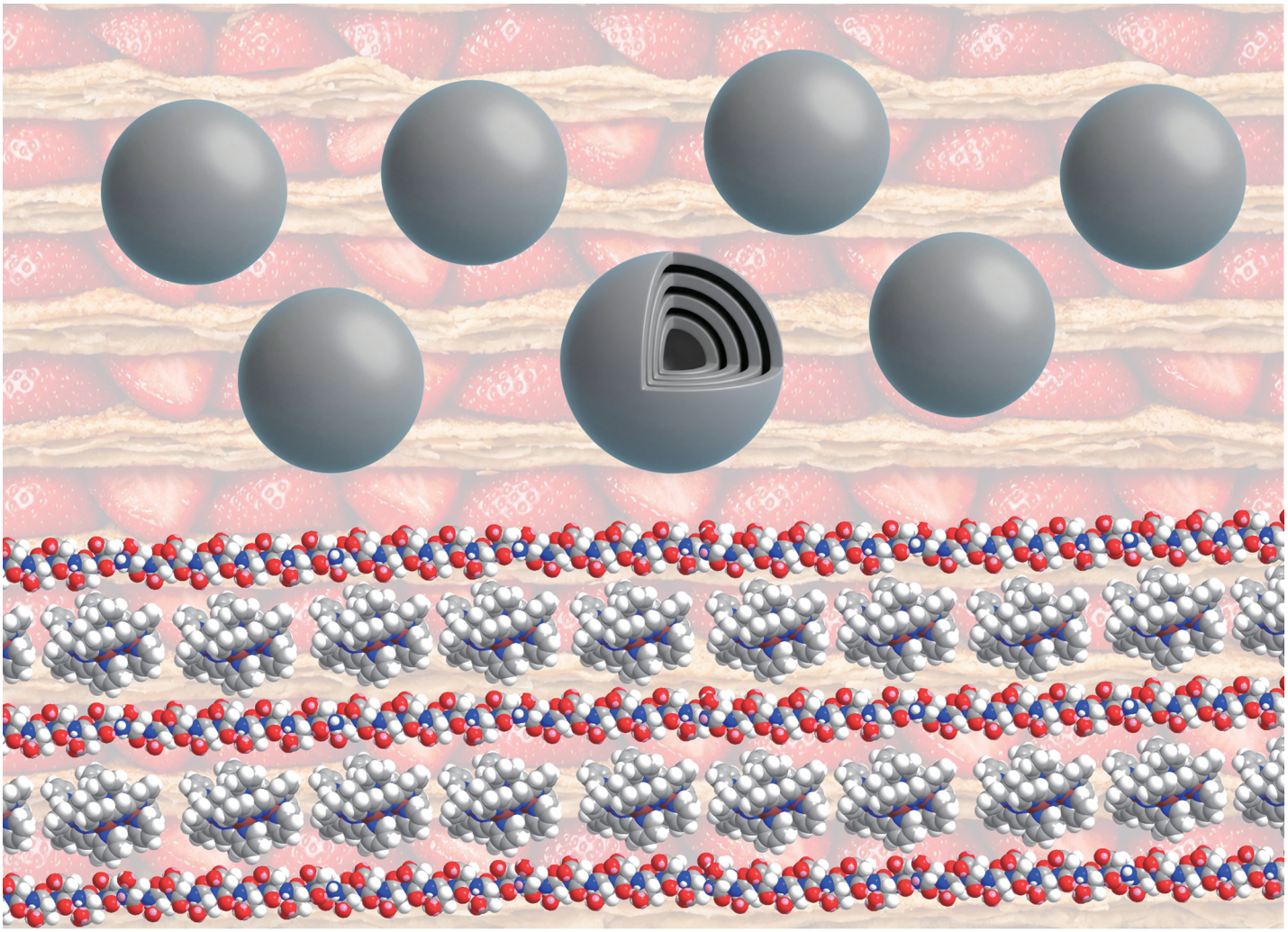

Showcasing research from Professor Kuroiwa's laboratory, Department of Nanoscience, Faculty of Engineering, Sojo University, Kumamoto, Japan.

Supramolecular hybrid of Fe pentanuclear complex/diblock copolypeptide amphiphiles with pH-responsive nano/microstructures in water

This work reports a supramolecular hybrid formed by co-assembling a pentanuclear iron (**Fe5**) complex with amphiphilic diblock copolypeptides in water. The peptide framework stabilizes the intact **Fe5** cluster and drives pH-responsive self-assembly into nano- and microstructured morphologies such as vesicles and lamellae. These hierarchical architectures modulate the spectroscopic and electrochemical properties of the **Fe5** complex, demonstrating how peptide-based supramolecular design enables functional metal complexes to operate effectively in aqueous environments.

Image reproduced by permission of Keita Kuroiwa from *Mater. Adv.*, 2026, **7**, 2039.

As featured in:

See Keita Kuroiwa *et al.*, *Mater. Adv.*, 2026, **7**, 2039.

ROYAL SOCIETY OF CHEMISTRY

rsc.li/materials-advances

Registered charity number: 207890

Materials Advances

ROYAL SOCIETY OF CHEMISTRY

PAPER

View Article Online
View Journal | View Issue

Cite this: *Mater. Adv.*, 2026, 7, 2039

Supramolecular hybrid of Fe pentanuclear complex/diblock copolypeptide amphiphiles with pH-responsive nano/microstructures in water

Keita Kuroiwa, *[a] Touka Tada,[a] Miki Ichise[a] and Shigeyuki Masaoka [b]

A pentanuclear iron (**Fe5**) complex was successfully co-assembled with an amphiphilic diblock copolypeptide in aqueous solution, forming well-organized supramolecular aggregates that exhibit distinct spectroscopic and redox properties. The hybrids adopted pH-responsive morphologies ranging from vesicle-like structures to micron-scale sheets, as confirmed by dynamic light scattering (DLS), scanning electron microscope (SEM), and transmission electron microscope (TEM) analyses. These measurements demonstrated that pH-dependent changes in aggregation state directly influence the redox behavior of the **Fe5** complex. Cyclic voltammetry (CV) revealed that hybrids incorporating longer poly(L-aspartic acid) segments and shorter poly(L-leucine) segments displayed enhanced water accessibility and ion transport, resulting in pronounced pH-dependent redox shifts. Vesicle-like structures, in particular, facilitated greater interaction between the metal centers and the aqueous environment, thereby promoting redox activity. Collectively, these findings demonstrate that the self-assembled peptide matrix regulates both the oxidation state and electrochemical response of the pentanuclear iron complex. This work highlights a promising strategy for tuning supramolecular environments to modulate catalytic behavior and provides a foundation for designing bioinspired polypeptide–metal complex hybrid systems capable of improving electrocatalytic water oxidation and oxygen evolution efficiency.

Received 2nd December 2025,
Accepted 8th January 2026

DOI: 10.1039/d5ma01393c

rsc.li/materials-advances

Introduction

The interactions between peptides (proteins) and metal complexes are crucial motifs in many biological systems, such as metalloproteins, where they facilitate synergistic supramolecular assemblies.[1–10] In natural systems, these processes often involve dissipative mechanisms, such as the self-assembly of oxygen carriers. These biological concepts have inspired generations of materials scientists to develop responsive and adaptive materials based on self-assembling polypeptides with metal complexes formed through both covalent and non-covalent interactions.[11]

In particular, advances in understanding the principles of hierarchical ordering at the micro- and mesoscopic levels, together with macroscopic functional control, have enabled the rational design of adaptive supramolecular polypeptide–metal hybrid materials.[12] A prominent and widely adopted approach involves forming architectures in aqueous environments through the interplay of hydrophobic and hydrophilic domains. The resulting assemblies are stabilized by cooperative and reversible interactions such as hydrogen bonding, electrostatic forces, host–guest interactions, metal–ligand coordination, hydrophobic interactions, and π–π stacking. Multiple hydrogen bonds and π–π stacking not only stabilize the supramolecular structures but also induce highly directional, high-aspect-ratio assemblies.[13–17]

Peptides incorporating metal complexes are particularly well suited for creating responsive materials that function in biologically relevant aqueous environments, owing to their intrinsic and tunable driving forces for forming extended, ordered structures.[18] Furthermore, these peptide-based superstructures exhibit biocompatibility and desirable functional properties for medical and catalytic applications.[19] Diblock copolypeptide amphiphiles are especially versatile in controlling supramolecular structures, depending on factors such as the combination of hydrophilic and hydrophobic amino acids, the degree of polymerization, and the balance between the two domains.[20–22] Their ability to form hydrogels and interact with various guest molecules allows the creation of functional and stimuli-responsive soft materials.[23,24]

To broaden the application of multi-stimulus-responsive peptides, we focused on their interactions with metal complexes. Based on the self-assembly behavior of diblock

[a] *Department of Nanoscience, Faculty of Engineering, Sojo University, 4-22-1 Nishi-ku, Kumamoto 860-0082, Japan. E-mail: keitak@nano.sojo-u.ac.jp*
[b] *Division of Applied Chemistry, Graduate School of Engineering, Osaka University, 2-1 Yamadaoka, Suita, Osaka 565-0871, Japan*

copolypeptide amphiphiles, it is possible to spatially organize hydrophilic and hydrophobic metal complexes in a defined sequence.[25–28] By exploiting the magnetic transitions, luminescence control, and redox properties of metal complexes, highly directional polypeptide/metal hybrid assemblies can be constructed, with tunable magnetic and electrochemical properties depending on the metal centers. Previous studies have demonstrated the ability to control physical properties in such supramolecular assemblies; however, interactions with small molecular metal complexes require a molecular design that preserves the intrinsic self-assembly properties of the polypeptide. In such designs, the balance between hydrophilic and hydrophobic domains is critical to maintaining structural integrity and responsiveness.

In this context, we selected the diblock copolypeptide amphiphile poly(L-aspartate)-*block*-poly(L-leucine) ($(Asp)_m$-*b*-$(Leu)_n$) as a versatile molecular scaffold. The hydrophilic aspartate residues provide multiple coordination sites through carboxylate groups, while the hydrophobic leucine segment forms α-helical secondary structures that drive hierarchical self-assembly. This combination enables both solubilization and spatial control of metal complexes within well-defined nanostructures in water.

Oligonuclear metal complexes, as key motifs of catalytic metal centers, are of particular interest due to their ability to facilitate electron transfer and metal–metal interactions.[29–31] Among them, the synthetic pentanuclear iron complex $[Fe^{II}_3Fe^{III}_2(\mu_3\text{-}O)(\mu\text{-}L)_6]^{3+}$ (**Fe5**; L = 3,5-bis(pyridyl)pyrazole) (Fig. 1 left) represents an archetypal redox-active cluster.[32] This complex possesses D_3 symmetry and a trigonal-bipyramidal framework, in which three equatorial Fe ions are bridged to two axial Fe centers through μ-oxo and μ-hydroxo linkages. Such a geometry allows flexible valence interconversion between Fe(II), Fe(III), and Fe(IV) states, resulting in efficient intramolecular electron transfer and high catalytic activity toward oxygen evolution. The **Fe5** complex functions as a robust and selective oxygen evolution catalyst under electrochemical conditions, exhibiting a current conversion efficiency of approximately 90% and an exceptional turnover frequency of 1900 s^{-1}. These features make **Fe5** an attractive building block for constructing redox-active supramolecular systems that mimic natural metalloenzymes.

Despite these advantages, **Fe5** complexes suffer from inherent limitations such as poor solubility in water and the formation of racemic mixtures, which hinder their applicability in aqueous or chiral environments. To address these challenges, we sought to hybridize **Fe5** clusters with amphiphilic diblock polypeptides that can provide both solubilization and chiral induction. The aspartate residues are expected to coordinate to the Fe centers, improving dispersion in aqueous media, while the α-helical leucine segments introduce chiral asymmetry and guide the supramolecular organization of the complex.

In this study, we report the design of a multicomponent self-assembling system comprising hydrophobic **Fe5** clusters and $(Asp)_m$-*b*-$(Leu)_n$ diblock copolypeptide amphiphiles (Fig. 1 right). This molecular architecture allows the spatial arrangement of **Fe5** complex within the peptide matrix, enabling modulation of their redox behavior and the formation of hierarchical nanostructures in aqueous environments. The resulting self-assembled hybrid materials exhibit tunable redox properties and chiral organization, offering a new strategy for developing supramolecular metalloprotein mimetics that integrate catalytic activity, chirality, and aqueous processability.

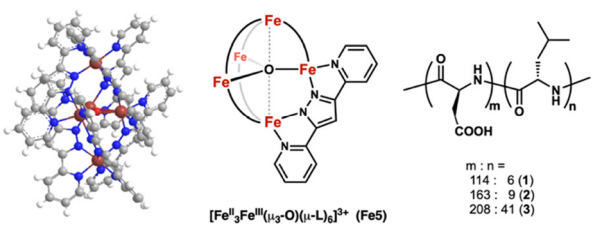

Fig. 1 Schematic illustration from crystal structure of **Fe5** and Chemical structure and illustration of Fe pentanuclear complex $[Fe^{II}_3Fe^{III}(\mu_3\text{-}O)(\mu\text{-}L)_6]^{3+}$ (**Fe5**) and diblock copolypeptide amphiphiles consisting of aspartate and leucine ($(Asp)_m$-*b*-$(Leu)_n$ **1–3**).

Experimental

The polypeptides, **Fe5** complexes, hybrid assemblies, and all reagents used in this study were prepared according to previously reported methods, as described in earlier publications (refer to the Supporting Information for details; Fig. S1–S7 and Table S1). ^{1}H NMR spectra were acquired using an ESC 400 (JEOL Ltd Tokyo, Japan). FT-IR measurements were obtained on a Spectrum 65 FT-IR (PerkinElmer, Inc., Waltham, MA, USA). Gel permeation chromatography/light scattering (GPC/LS) was performed at 60 °C using a Shimadzu LC solution GPC system incorporating a RID-10A differential refractometer detector and a CBM-20A pump/controller (Shimadzu Co., Ltd Kyoto, Japan). Separations were achieved using 10^5, 10^3 Å, and 500 Å Phenomenex Phenogel 5 μm columns with 0.1 M LiBr in DMF as the eluent and sample concentrations of 1 mg mL^{-1}. Pyrogen-free deionized water was obtained from Direct-Q3-UV (Merck KGaA, Darmstadt, Germany) purification units. Transmission electron microscopy (TEM) was performed using a Titan Themis 200 (Thermo Fisher Scientific Co. Ltd, Waltham, MA, USA) operating at 200 kV. TEM samples were prepared by transferring the surface layers of solutions to carbon-coated grids (Okenshoji Co., Ltd, Tokyo, Japan). Scanning electron microscopy (SEM) was carried out with an ERA-600 microscopy (Elionix Inc. Tokyo, Japan) operating at 20 kV. Scanning electron microscope samples were prepared by transferring the surface layers of dispersions to Cu plate. DLS measurements were acquired using an DLS-6000 with He-Ne laser (Otsuka Electronics Co., Ltd Osaka, Japan). Inductively coupled plasma optical emission spectroscopy (ICP-OES) data were obtained with an iCAP 7400 instrument (Thermo Fisher Scientific Co. Ltd, Waltham, MA, USA). UV-visible spectra were obtained using RF-2500PC spectrophotometer (Shimadzu Co., Ltd, Kyoto, Japan). Circular dichroism (CD) spectra were recorded on a J-820 spectropolarimeter (JASCO Corp., Tokyo, Japan) using a 0.1 mm pathlength quartz cylindrical cell. The measurements

were performed with a bandwidth of 1.0 nm and a scan speed of 200 nm min^{-1}. An CV-50W potentiostat analyzer (ALS Co. Ltd, Tokyo, Japan) was used for the electrochemical measurements, which were carried out at room temperature in a three-electrode cell. A glassy carbon (GC) rod (diameter 3 mm, geometric area 0.071 cm^2) implanted in polyether ether ketone (PEEK) was purchased from BAS Inc. (Tokyo, Japan). The GC electrode was used as the working electrode, and a Pt wire and an Ag/AgCl (KCl saturated) electrode were used as the counter and reference electrodes, respectively. The electrode was immersed in dispersion of [**Fe5**] = 0.1 mM in 0.5 M KCl aqueous solution, and cycled several times between a potential of −0.40 and 1.10 V until a steadystate voltammogram was reached.

Results and discussion

Preparation of hybrids

The hybrid **Fe5** complex/diblock copolypeptide amphiphiles were prepared at a metal complex concentration of 0.1 mM. The pentanuclear Fe complex and each anionic diblock copolypeptide amphiphile were first measured separately in sample tubes to achieve a 3 : 10 molar ratio of the **Fe5** complex to aspartic acid residues. To prepare the aqueous polymer solution, 10 mL of deionized water was added to the tube containing the anionic diblock copolypeptide amphiphile. This polymer solution was then transferred to the tube containing the **Fe5** complex under gentle stirring to form hybrid samples **1–3**. The resulting mixtures were purified by dialysis to remove any unreacted or undissolved species. The dialyzed solutions were subsequently lyophilized, and the obtained solids were redissolved in 2 mL of water to afford aqueous solutions of the hybrids (**1**: Asp_{114}-*b*-Leu_6, **2**: Asp_{163}-*b*-Leu_9, and **3**: Asp_{208}-*b*-Leu_{41}). All prepared hybrids (**1–3**/**Fe5**) were systematically characterized by elemental analysis and ICP-OES measurements (see Supplementary Information, and Table S2). These analyses confirmed that the hybrids were formed with an Asp-to-**Fe5** molar ratio of precisely 10 : 3, consistent with the intended composition. The well-defined and reproducible Fe contents indicate that the **Fe5** complexes are incorporated into the diblock copolypeptide matrices without undergoing significant structural degradation or fragmentation during hybrid formation. The molecular integrity of the **Fe5** complex within the hybrids is further corroborated in subsequent sections by UV–vis absorption and CD spectroscopy following the discussion of the nanostructures, and their electrochemical properties are examined in detail later by cyclic voltammetry (CV).

For each hybrid (**1–3**)/**Fe5** sample, the pH of the aqueous solution was adjusted to 4, 7, or 10 using 0.1 M NaOH or 0.1 M HCl solutions. In all cases, the resulting aqueous solutions exhibited slight turbidity, suggesting the formation of colloidal supramolecular assemblies. Further characterization of these assemblies by electron microscopy and DLS is described in the following sections.

Structural characterization of hybrids

TEM images of the pH-dependent aqueous samples of the complexes are shown in Fig. 2. In **1**/**Fe5**, sheet-like aggregated

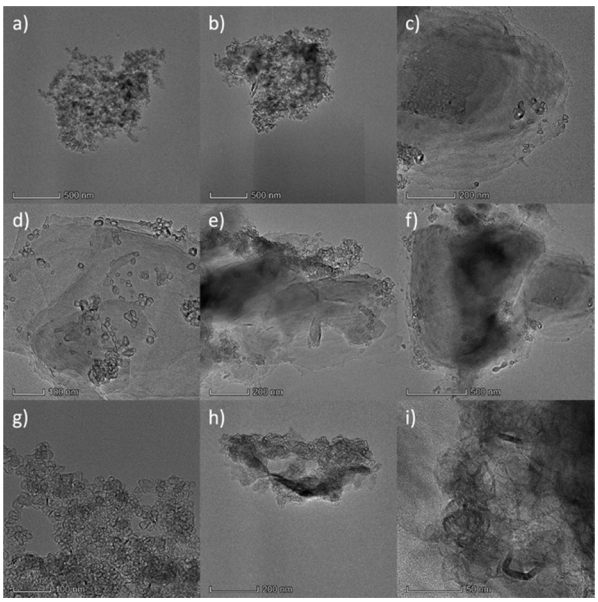

Fig. 2 TEM image for hybrids of (a) **1**/**Fe5** at pH 4, (b) **1**/**Fe5** at pH 7, (c) **1**/**Fe5** at pH 10, (d) **2**/**Fe5** at pH 4, (e) **2**/**Fe5** at pH 7, (f) **2**/**Fe5** at pH 10, (g) **3**/**Fe5** at pH 4, (h) **3**/**Fe5** at pH 7, (i) **3**/**Fe5** at pH 10, where [Fe complex] = 0.1 mM.

structures several micrometers in width were observed (Fig. 2a–c). At pH 4 (Fig. 2a) and pH 7 (Fig. 2b), vesicle-like domains with diameters of approximately 100 nm were found within these sheets, whereas at pH 10, the sheets exhibited several internal vesicular structures (Fig. 2c). Similar morphological trends were observed for **2**/**Fe5** (Fig. 2d–f). In contrast, **3**/**Fe5** showed a significantly higher abundance of vesicle-like structures at pH 4 (Fig. 2g) and pH 7 (Fig. 2h). Particularly at these pH values, vesicles with diameters around 500 nm aggregated to form continuous film-like assemblies. At pH 10, irregular polymer film structures several micrometers in size were observed (Fig. 2i).

Among the hybrids, **3**/**Fe5** displayed vesicle- and sheet-like morphologies with greater rigidity compared to **1**/**Fe5** and **2**/**Fe5**. This enhanced stiffness is likely attributed to the longer hydrophilic Asp and hydrophobic Leu segments, which promote both intermolecular and hydrophobic interactions. Owing to these distinct structural characteristics, a more detailed examination of **3**/**Fe5** was conducted (Fig. 3). At pH 4, multilamellar vesicles exhibiting a lamellar pattern with layer thicknesses of approximately 30–50 nm and interlayer spacings of about 3 nm were observed (Fig. 3a). X-ray crystallographic data of the **Fe5** complex indicate a lattice constant of 30 Å (3.0 nm) along the *c*-axis,[32] suggesting that the peptide assemblies encapsulate the metal complexes to form multilayered vesicle-like structures. Based on the chain length of peptide **3**, a β-sheet in the all-trans conformation would extend to ∼40 nm, while an α-helix would measure ∼26 nm, implying that a single peptide molecular layer can incorporate multiple layers of metal complexes (discussed later). With increasing pH (Fig. 3b and c), the lamellar order became progressively disordered, leading to the formation of sheet-like films as the

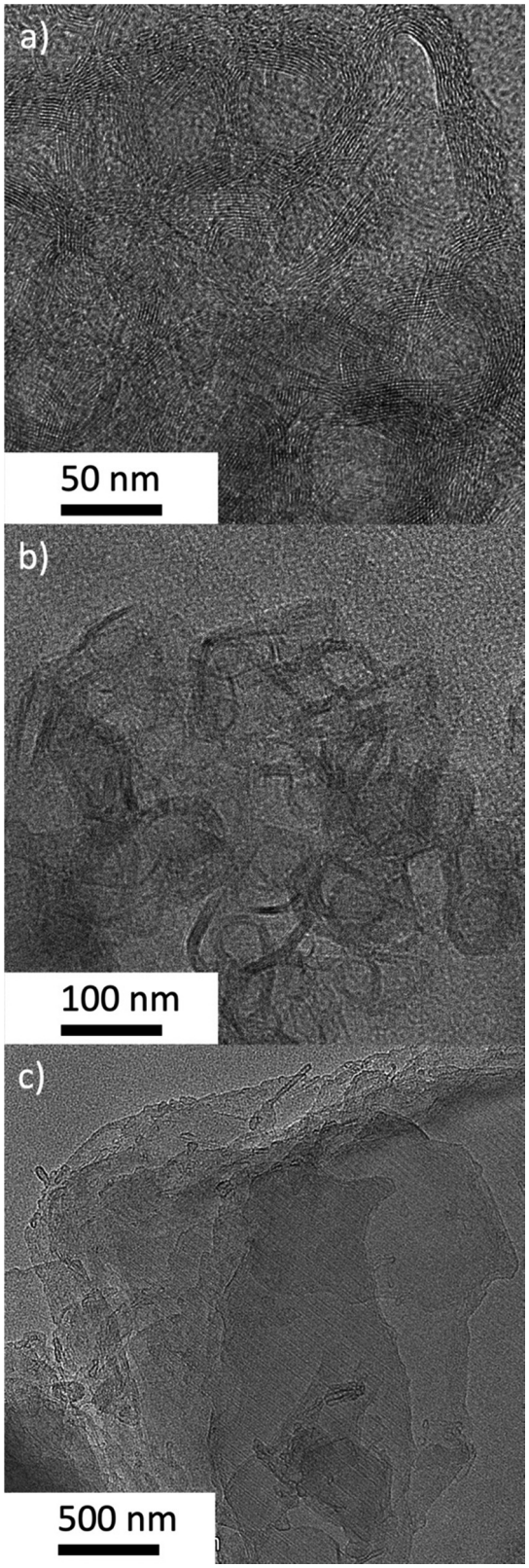

Fig. 3 HR-TEM image for hybrids of (a) **3/Fe5** at pH 4, (b) **3/Fe5** at pH 7, (c) **3/Fe5** at pH 10, where [Fe complex] = 0.1 mM.

interlayer spacing diminished and eventually disappeared. These results indicate that protonation and deprotonation of aspartic acid residues modulate the coordination environment of **Fe5** complexes, driving a morphological transition from vesicle-like to sheet-like structures.

SEM images of the freeze-dried samples are shown in Fig. S8. Consistent with TEM observations, all hybrids exhibited sheet-like aggregates ranging from a few to several tens of micrometers in size. For **1/Fe5** and **2/Fe5**, fragmented sheet-like structures were predominant at pH 4 (Fig. S8a and d), whereas smoother, more continuous sheets were observed as the pH increased (Fig. S8). In **3/Fe5**, granular structures coalesced into larger, smoother sheets at higher pH, corroborating the vesicle-to-sheet transformation observed in TEM. Further elemental mapping by scanning transmission electron microscopy coupled with energy-dispersive X-ray spectroscopy (STEM–EDS) revealed that the sheet-like structures contained substantial amounts of carbon (C), nitrogen (N), and oxygen (O) from the peptide components, as well as iron (Fe) from the metal complexes (Fig. S9–S11). These results confirm that the observed assemblies are hybrid structures composed of both peptides and **Fe5** complexes, self-assembled in aqueous environments.

The size distribution of the aqueous microstructures was further examined by DLS at room temperature (Fig. 4 and Table 1). The pH 4 samples exhibited monodisperse distributions with hydrodynamic diameters of 150–250 nm, corresponding well to the vesicular structures observed in TEM. As the pH increased to 7 and 10 for **2/Fe5** and **3/Fe5**, the DLS profiles gradually shifted from monodisperse to polydisperse, with larger structures up to several micrometers detected at pH 10. These results strongly support the formation of micrometer-scale sheet-like aggregates in aqueous media, consistent with the morphological evolution observed by electron microscopy.

Physicochemical properties of hybrids

The UV–vis spectra of the hybrids exhibited distinct responses to pH variation (Fig. 5). For **1/Fe5**, absorption peaks were observed at 200–300 nm and 350–550 nm (Fig. 5a). The **Fe5**$(BF_4)_3$ complex is known to show four characteristic spectral stages corresponding to oxidation from the S_0 to S_4 states.[32] In the S_0 state, a strong band appears around 400 nm, attributed to the metal-to-ligand charge transfer (MLCT) transition of the low-spin Fe(II) ion. In the hybrid **1/Fe5**, little spectral change was detected upon pH variation, suggesting limited redox flexibility.

In contrast, **2/Fe5** exhibited a gradual decrease in absorbance near 400 nm, with an isosbestic point at 558 nm (Fig. 5b), indicating a pH-dependent equilibrium between redox states. The changes were more pronounced for **3/Fe5** (Fig. 5c), where the 400 nm band—prominent at pH 7 and 10—almost disappeared at pH 4. During oxidation from S_0 to S_1, small spectral shifts indicated oxidation of the high-spin Fe(II) site, while the transition from S_1 to S_2 caused the 400 nm band to vanish, reflecting the predominance of Fe(III).[32] These results clearly demonstrate pH-dependent oxidation behavior. Morphological observations revealed vesicle-like structures forming at lower pH, suggesting that such assemblies provide a favorable

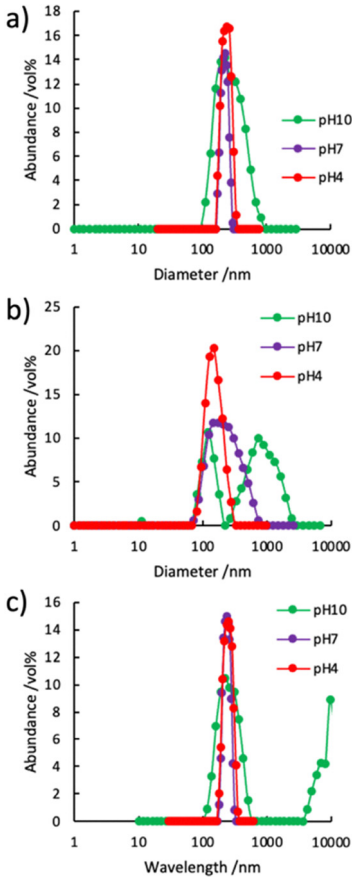

Fig. 4 DLS measurement for hybrids of (a) **1/Fe5**, (b) **2/Fe5**, and (c) **3/Fe5**, prepared by the samples at different pH, where [Fe complex] = 0.1 mM.

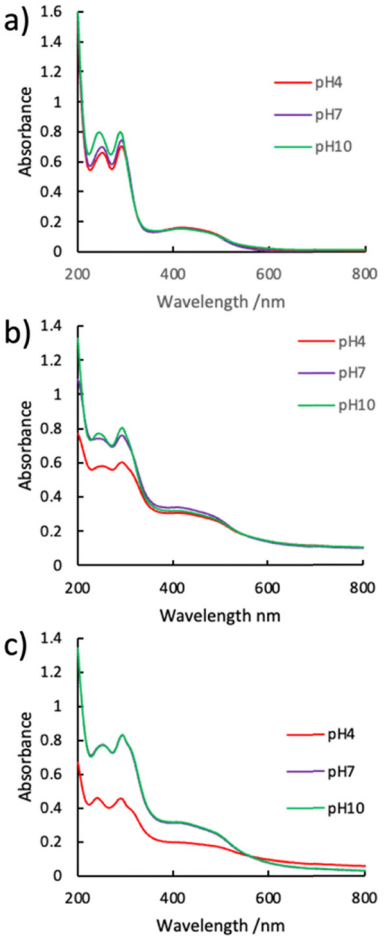

Fig. 5 UV-vis spectra for hybrids of (a) **1/Fe5**, (b) **2/Fe5**, and (c) **3/Fe5**, prepared by the samples at different pH, where [Fe complex] = 0.1 mM.

Table 1 Maximum and average sizes in volume-based size distributions obtained from dynamic light scattering in Fig. 4

	pH	Peak/nm	Average/nm
1/Fe5	pH4	230	245
	pH7	225	284
	pH10	241	520
2/Fe5	pH4	149	184
	pH7	175	325
	pH10	121, 893	1345
3/Fe5	pH4	251	314
	pH7	236	297
	pH10	223, 9543	6352

microenvironment for oxidation in aqueous media. This effect was particularly evident for **3/Fe5**, where both pH variation and morphological transformation accelerated oxidation.

The CD spectra provided insights into peptide secondary structures and their relationship to morphology (Fig. 6). For **1/Fe5**, a positive Cotton effect around 190–200 nm—characteristic of β-sheet conformations[33–36]—was observed at pH 4 (Fig. 6a). As pH increased, this signal diminished, consistent with a transition toward random coil structures. For **2/Fe5** and **3/Fe5**, a positive Cotton effect near 195 nm and a negative one near 205 nm were observed at pH 4 (Fig. 6b and c), indicating α-helical characteristics.[37–40] With increasing pH, the negative band intensified, implying a gradual loss of α-helicity and the emergence of random coil components. Correlating these findings with morphological observations suggests that vesicle-like structures are associated primarily with α-helical conformations, whereas sheet-like aggregates correspond to random coil and β-sheet structures. In the extended CD spectra (190–900 nm), weak induced circular dichroism (ICD) bands appeared around 500 nm for **2/Fe5** and **3/Fe5** at pH 4 (Fig. 6e and f). These ICD signals likely originate from exciton coupling between the chiral peptide environment and the metal complex, implying strong peptide–metal interactions under acidic conditions that may promote vesicle formation and enhance redox activity.

CV measurements were conducted in 0.1 M $NaClO_4$ aqueous solution at a scan rate of 10 mV s^{-1} (Fig. 7). Because the pentanuclear **Fe5** complex is insoluble in water, its intrinsic redox properties have been established primarily in organic solvents such as acetonitrile, where three reversible redox couples are observed at approximately 0.13, 0.30, and 0.68 V *vs.* Fc/Fc^+. These redox processes are assigned to successive one-electron transitions of the intact **Fe5** core, namely

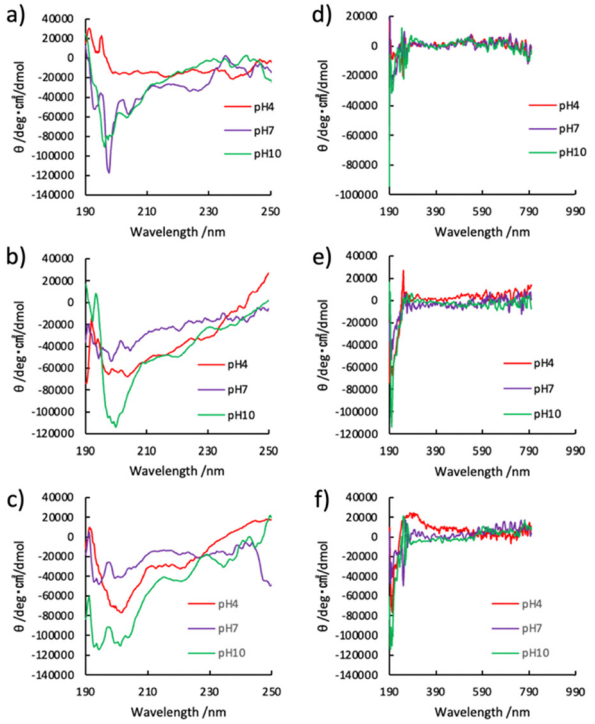

Fig. 6 CD spectra for hybrid of (a) **1/Fe5**, (b) **2/Fe5**, and (c) **3/Fe5**, prepared by the samples at different pH, where [Fe complex] = 0.1 mM. CD spectra over a broader range (190–900 nm, (d) **1/Fe5**, (e) **2/Fe5**, and (f) **3/Fe5**) show a slight induced circular dichro-ism (ICD) around 500 nm for **2/Fe5** and **3/Fe5** at pH 4.

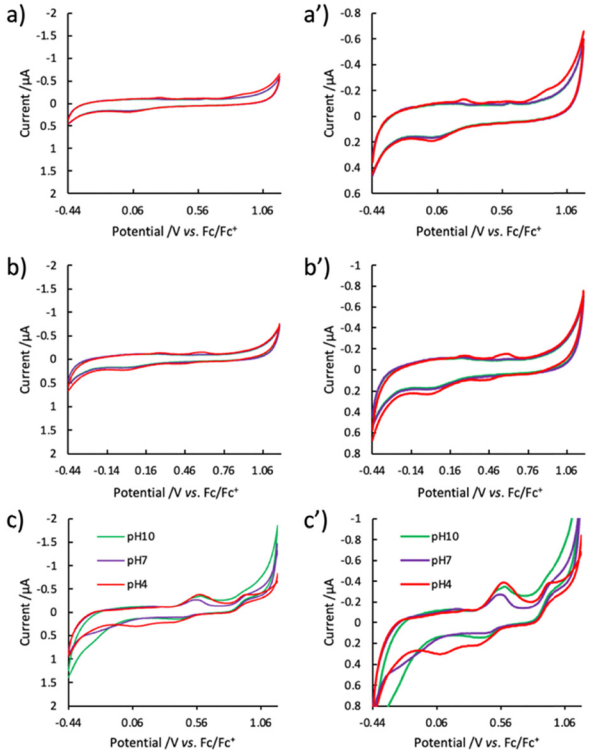

Fig. 7 Cyclic voltammograms (CV) in 0.1 M $NaClO_4$ for hybrids of (a) **1/Fe5**, (b) **2/Fe5**, and (c) **3/Fe5**, prepared by the samples at different pH, where [Fe complex] = 0.1 mM. The sweep rate was 10 mV s^{-1}. Panels (a′)–(c′) show enlarged views of the corresponding CVs in (a)–(c), respectively, with expanded current (vertical) axes to highlight electrochemical features.

$Fe^{II}_4Fe^{III}_1 \rightleftarrows Fe^{II}_3Fe^{III}_2$, $Fe^{II}_3Fe^{III}_2 \rightleftarrows Fe^{II}_2Fe^{III}_3$, and $Fe^{II}_2Fe^{III}_3 \rightleftarrows Fe^{II}_1Fe^{III}_4$, respectively.[32] In the present aqueous peptide–**Fe5** hybrid systems, oxidation waves at potentials close to these characteristic values were observed, particularly under acidic conditions (pH 4), indicating that the multinuclear **Fe5** framework remains intact after hybrid formation. Importantly, UV–vis absorption spectra of all hybrids exhibited nearly identical absorbance intensities and spectral profiles corresponding to the **Fe5** complex, irrespective of peptide composition or pH conditions. This observation strongly supports that the **Fe5** complexes are not decomposed or leached from the assemblies in water, but are preserved within the peptide matrix in comparable concentrations across all hybrid systems.

The electrochemical response, however, showed a pronounced dependence on supramolecular morphology. Among the hybrids, **3/Fe5** displayed markedly enhanced redox currents, particularly at pH 4, whereas **1/Fe5** and **2/Fe5** exhibited smaller and less pH-dependent currents. TEM and STEM analyses revealed that **3/Fe5** forms multilayered vesicle-like assemblies under acidic conditions, while the other hybrids tend to form more compact or fragmented sheet-like structures. These multilayered vesicles are expected to provide interconnected aqueous domains and ion-permeable pathways, allowing water molecules and electrolyte ions to access the embedded **Fe5** complexes more efficiently.

Rather than being completely buried within a dense peptide matrix, the **Fe5** complexes in **3/Fe5** are likely distributed along hydrated interlayers or near internal aqueous interfaces of the multilayer vesicles, enabling smooth ion exchange and electron transfer at the electrode interface. In contrast, in **1/Fe5** and **2/Fe5**, stronger confinement within less hydrated peptide domains likely limits electronic communication and suppresses the observed current intensities. Regarding the potential degradation of peptide structures under oxidative conditions, the observed stability of the UV–vis and CD spectral features, together with the reproducibility of CV responses across repeated scans, indicates that the diblock copolypeptide framework remains structurally stable within the investigated potential window. Moreover, the amphiphilic nature of the diblock copolypeptide amphiphiles enables dynamic yet robust self-assembly, allowing local structural rearrangements without catastrophic degradation, even under electrochemically active conditions. These results demonstrate that the redox activity of the **Fe5** complex in water is governed not only by its intrinsic electronic structure but also by the supramolecular architecture of the peptide assembly. In particular, the multilayered vesicle-like structures formed by **3/Fe5** at pH 4 provide a favorable microenvironment that balances structural stability, water accessibility, and electronic communication, thereby enabling smoother electrochemical activation of the intact **Fe5** complex in aqueous media.

Combined UV–vis, CV, and DLS results suggest molecular alignment of the metal complexes within the polypeptide framework. TEM observations revealed vesicular nanostructures with

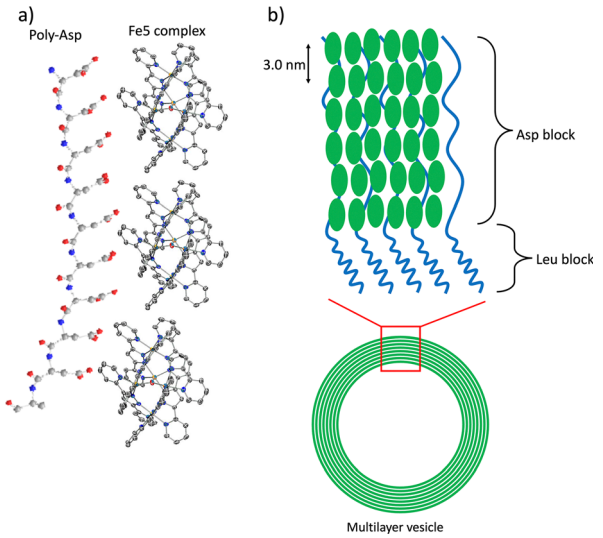

Fig. 8 Hierarchical schematic illustration of the self-assembly of diblock copolypeptide amphiphiles **3/Fe5**, showing how diblock copolypeptide amphiphiles with Fe pentanuclear complexes (a) form a vesicular-like structure (b).

organized **Fe5** arrangements, indicating that peptide–metal interactions dictate supramolecular ordering. The **Fe5** cluster's oxidation states are highly sensitive to environmental conditions, suggesting adaptable 1D or 2D packing arrangements. Elemental analysis confirmed that the optimal hybrid composition corresponds to a 3 : 10 ratio of **Fe5** complex to diblock copolypeptide amphiphile, which maximizes solubility and promotes stable self-assembly. Crystallographic analysis indicates that **Fe5** complexes form compact 1D chains along the c-axis with loose intermolecular packing (~30 Å spacing), consistent with the periodicity of carboxyl groups in β-sheeted, or random coiled poly(L-aspartic acid), as predicted by AlphaFold2 and confirmed *via* PyMOL simulations (Fig. S12).[41,42] These results support the hypothesis that the **Fe5**–peptide interactions arise from a delicate balance between β-sheet-rich amphiphilic polypeptides and the flexible **Fe5** clusters. The lengths of the poly(L-aspartic acid) and poly(L-leucine) blocks play critical roles in determining the nanoscale structure and redox properties of the hybrids. Variations in block length modulate metal–peptide interactions, ion-transport activation energies, and overall electrochemical behavior. Therefore, the redox activity of the **Fe5** cluster complexes is governed by peptide-mediated self-assembly dynamics, which control structural phase transitions and electron transfer within the **Fe5** network (Fig. 8).

Conclusions

In this study, we successfully demonstrated the aqueous self-assembly of a redox-active pentanuclear iron complex (**Fe5**), known for its high catalytic stability in oxygen evolution, with amphiphilic diblock copolypeptides composed of aspartic acid and leucine. The resulting hybrid system enabled the formation of well-organized supramolecular architectures in water—ranging from vesicle-like to sheet-like structures—whose morphology and oxidation state were both tunable by pH.

The **Fe5** complex, possessing multiple accessible oxidation states, was efficiently incorporated into peptide-based assemblies, overcoming its intrinsic water insolubility and racemic nature. Structural analyses by TEM, SEM, and DLS revealed that at lower pH, multilayered vesicle-like morphologies were predominant, whereas at higher pH, these transformed into extended sheet-like aggregates. These morphological transitions were closely correlated with the Fe oxidation state and the redox response observed in UV–vis and cyclic voltammetry measurements.

Furthermore, circular dichroism spectroscopy indicated that α-helical peptide conformations favored vesicle formation, while random coil and β-sheet structures corresponded to sheet-like assemblies. These findings suggest that pH-dependent protonation of aspartic acid residues modulates peptide–metal interactions, thereby controlling both supramolecular morphology and redox behavior. The length and hydrophobic balance of the diblock copolypeptide segments were also found to be key parameters in tuning aggregation, redox activity, and structural organization.

Overall, the present study demonstrates that hybridization of diblock polypeptide amphiphiles with redox-active multinuclear metal complexes enables precise structural and electronic control in aqueous environments. This approach provides a promising design strategy for constructing artificial metalloprotein-like systems, where cooperative peptide–metal interactions may facilitate water oxidation and electron transfer. Further optimization of water molecule transport within the peptide matrix is expected to advance this system toward biomimetic catalysts capable of enhancing electrocatalytic oxygen evolution efficiency.

Author contributions

K. K., T. T., M. I., and S. M. developed the methodology and performed the experimental investigations and validation. The manuscript was written through contributions of K. K. and S. M. All authors have given approval to the final version of the manuscript.

Conflicts of interest

There are no conflicts to declare.

Data availability

All data supporting the findings of this study are available within the article and its supplementary information (SI) files. Supplementary information: materials and instrumentation, general polypeptide synthesis, general preparation of hybrids, SEM, and HR-STEM EDX are available. See DOI: https://doi.org/10.1039/d5ma01393c.

Acknowledgements

This work was financially supported in part by Grants-in-Aid for Scientific Research on Innovative Areas (New Polymeric Materials Based on Element Blocks, no. 2401) (no. 25102547 and 15H00770). K.K. is also grateful for the financial support of the Canon Foundation (grant no. K16-0146), for the Izumi science and technology foundation (grant no. 2024-J-015), and for a research grant from Sojo University (grant no. RT02000003).

Notes and references

1 E. C. Theil and K. N. Raymond, in *Bioinorganic Chemistry*, ed. I. Beritini, H. B. Gray, S. J. Lippard and J. S. Valentine, University Science Books, Mill Valley, Calif, CA, USA, 1994, pp. 1–35.
2 R. H. Holm, P. Kennepohl and E. I. Solomon, *Chem. Rev.*, 1996, **96**, 2239–2314.
3 J. R. Winkler and H. B. Gray, *Chem. Rev.*, 2013, **114**, 3369–3380.
4 M. L. Zastrow and V. L. Pecoraro, *Coord. Chem. Rev.*, 2013, **257**, 2565–2588.
5 C. S. Mocny and V. L. Pecoraro, *Acc. Chem. Res.*, 2015, **48**, 2388–2396.
6 F. Nastri, M. Chino, O. Maglio, A. Bhagi-Damodaran, Y. Lu and A. Lombardi, *Chem. Soc. Rev.*, 2016, **45**, 5020–5054.
7 K. J. Grayson and J. L. R. Anderson, *Curr. Opin. Struct. Biol.*, 2018, **51**, 149–155.
8 V. Putignano, A. Rosato, L. Banci and C. Andreini, *Nucleic Acids Res.*, 2018, **46**, D459–D464.
9 A. Lombardi, F. Pirro, O. Maglio, M. Chino and W. F. DeGrado, *Acc. Chem. Res.*, 2019, **52**, 1148–1159.
10 T. Shimizu, D. Huang, F. Yan, M. Stranava, M. Bartosova, V. Fojtikova and M. Martinkova, *Chem. Rev.*, 2015, **115**, 6491–6533.
11 G. S. Ghodake, S. K. Shinde, R. G. Saratale, A. A. Kadam, G. D. Saratale, A. Syed, F. Ameen and D. Y. Kim, *Beilstein J. Nanotechnol.*, 2018, **9**, 1414–1422.
12 J. Dong, Y. Liu and Y. Cui, *J. Am. Chem. Soc.*, 2021, **143**, 17316–17336.
13 R. Eelkema and A. Pich, *Adv. Mater.*, 2020, **32**, e1906012.
14 O. S. Stach, K. Breul, C. M. Berač, M. Urschbach, S. Seiffert and P. Besenius, *Macromol. Rapid Commun.*, 2021, **43**, 2100473.
15 P. Sharma, H. Kaur and S. Roy, *Biomacromolecules*, 2019, **20**, 2610–2624.
16 Y. Wang, H. Su, Y. Wang and H. Cui, *ACS Macro Lett.*, 2022, **11**, 1355–1361.
17 J. Li, J. Xu, X. Li, W. Gao, L. Wang, L. Wu, M. Lee and W. Li, *Soft Matter*, 2016, **12**, 5572–5580.
18 T. P. Vinod, S. Zarzhitsky, A. Morag, L. Zeiri, Y. Levi-Kalisman, H. Rapaport and R. Jelinek, *Nanoscale*, 2013, **5**, 10487–10493.
19 C. Diaferia, E. Gianolio and A. Accardo, *J. Pept. Sci.*, 2019, **25**, e3157.
20 D. J. Pochan, L. Pakstis, B. Ozbas, A. P. Nowak and T. J. Deming, *Macromolecules*, 2002, **35**, 5358–5360.
21 A. P. Nowak, V. Breedveld, L. Pakstis, B. Ozbas, D. J. Pine, D. Pochan and T. J. Deming, *Nature*, 2002, **417**, 424–428.
22 E. P. Holowka, V. Z. Sun, D. T. Kamei and T. J. Deming, *Nat. Mater.*, 2007, **6**, 52–57.
23 C. Y. Yang, B. Song, Y. Ao, A. P. Nowak, R. B. Abelowitz, R. A. Korsak, L. A. Havton, T. J. Deming and M. V. Sofroniew, *Biomaterials*, 2009, **30**, 2881–2898.
24 A. Rasines Mazo, S. Allison-Logan, F. Karimi, N. J. Chan, W. Qiu, W. Duan, N. M. O'Brien-Simpson and G. G. Qiao, *Chem. Soc. Rev.*, 2020, **49**, 4737–4834.
25 K. Kuroiwa, T. Arie, S. Sakurai, S. Hayami and T. J. Deming, *J. Mater. Chem. C*, 2015, **3**, 7779–7783.
26 A. Tsubasa, S. Otsuka, T. Maekawa, R. Takano, S. Sakurai, T. J. Deming and K. Kuroiwa, *Polymer*, 2017, **128**, 347–355.
27 Y. Tanimura, M. Sakuragi, T. J. Deming and K. Kuroiwa, *ChemNanoMat*, 2020, **6**, 1635–1640.
28 Y. Tanimura, K. Miyamoto, T. Shiga, M. Nihei and K. Kuroiwa, *J. Phys. Chem. C*, 2023, **127**, 16525–16537.
29 Z. Xu, F. S. Xiao, S. K. Purnell, O. Alexeev, S. Kawi, S. E. Deutsch and B. C. Gates, *Nature*, 1994, **372**, 346–348.
30 K. Endo, K. Tanaka, M. Ogawa and T. Shibata, *Org. Lett.*, 2011, **13**, 868–871.
31 L.-J. Wu, W. Lee, P. Kumar Ganta, Y.-L. Chang, Y.-C. Chang and H.-Y. Chen, *Coord. Chem. Rev.*, 2023, **475**, 214847.
32 M. Okamura, M. Kondo, R. Kuga, Y. Kurashige, T. Yanai, S. Hayami, V. K. Praneeth, M. Yoshida, K. Yoneda, S. Kawata and S. Masaoka, *Nature*, 2016, **530**, 465–468.
33 S. Zhang, C. Lockshin, R. Cook and A. Rich, *Biopolymers*, 1994, **34**, 663–672.
34 S. St. Pierre, R. T. Ingwall, M. S. Verlander and M. Goodman, *Biopolymers*, 2004, **17**, 1837–1848.
35 D. G. Osterman and E. T. Kaiser, *J. Cell. Biochem.*, 1985, **29**, 57–72.
36 A. Brack and L. E. Orgel, *Nature*, 1975, **256**, 383–387.
37 Y. Singh, P. C. Sharpe, H. N. Hoang, A. J. Lucke, A. W. McDowall, S. P. Bottomley and D. P. Fairlie, *Chem. – Eur. J.*, 2011, **17**, 151–160.
38 G. Seipke, H. A. Arfmann and K. G. Wagner, *Biopolymers*, 1974, **13**, 1621–1633.
39 W. B. Rippon, H. H. Chen and A. G. Walton, *J. Mol. Biol.*, 1973, **75**, 369–375.
40 E. Peggion, A. Cosani, M. Terbojevich and G. Borin, *Biopolymers*, 1972, **11**, 633–643.
41 J. Jumper, R. Evans, A. Pritzel, T. Green, M. Figurnov, O. Ronneberger, K. Tunyasuvunakool, R. Bates, A. Zidek, A. Potapenko, A. Bridgland, C. Meyer, S. A. A. Kohl, A. J. Ballard, A. Cowie, B. Romera-Paredes, S. Nikolov, R. Jain, J. Adler, T. Back, S. Petersen, D. Reiman, E. Clancy, M. Zielinski, M. Steinegger, M. Pacholska, T. Berghammer, S. Bodenstein, D. Silver, O. Vinyals, A. W. Senior, K. Kavukcuoglu, P. Kohli and D. Hassabis, *Nature*, 2021, **596**, 583–589.
42 M. Varadi, S. Anyango, M. Deshpande, S. Nair, C. Natassia, G. Yordanova, D. Yuan, O. Stroe, G. Wood, A. Laydon, A. Zidek, T. Green, K. Tunyasuvunakool, S. Petersen, J. Jumper, E. Clancy, R. Green, A. Vora, M. Lutfi, M. Figurnov, A. Cowie, N. Hobbs, P. Kohli, G. Kleywegt, E. Birney, D. Hassabis and S. Velankar, *Nucleic Acids Res.*, 2022, **50**, D439–D444.